JACS
JOURNAL OF THE AMERICAN CHEMICAL SOCIETY
Article
pubs.acs.org/JACS

Size Dependence of Steric Shielding and Multivalency Effects for Globular Binding Inhibitors

Jonathan Vonnemann,*[,‡] Susanne Liese,*[,†] Christian Kuehne,[∥] Kai Ludwig,[§] Jens Dernedde,[∥] Christoph Böttcher,[§] Roland R. Netz,[†] and Rainer Haag[‡]

[‡]Institute of Chemistry and Biochemistry, [†]Institute of Theoretical Physics, and [§]Research Centre of Electron Microscopy and Core Facility BioSupraMol, Institute of Chemistry and Biochemistry, Freie Universität Berlin, Berlin, Germany

[∥]Institute of Laboratory Medicine, Clinical Chemistry and Pathobiochemistry, Charité-Universitätsmedizin Berlin, Berlin, Germany

Supporting Information

ABSTRACT: Competitive binding inhibitors based on multivalent nanoparticles have shown great potential for preventing virus infections. However, general design principles of highly efficient inhibitors are lacking as the quantitative impact of factors such as virus concentration, inhibitor size, steric shielding, or multivalency effects in the inhibition process is not known. Based on two complementary experimental inhibition assays we determined size-dependent steric shielding and multivalency effects. This allowed us to adapt the Cheng−Prusoff equation for its application to multivalent systems. Our results show that the particle and volume normalized IC_{50} value of an inhibitor at very low virus concentration predominantly depends on its multivalent association constant, which itself exponentially increases with the inhibitor/virus contact area and ligand density. Compared to multivalency effects, the contribution of steric shielding to the IC_{50} values is only minor, and its impact is only noticeable if the multivalent dissociation constant is far below the virus concentration, which means if all inhibitors are bound to the virus. The dependence of the predominant effect, either steric shielding or multivalency, on the virus concentration has significant implications on the in vitro testing of competitive binding inhibitors and determines optimal inhibitor diameters for the efficient inhibition of viruses.

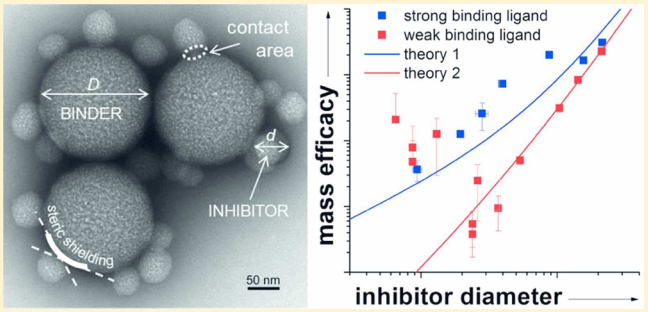

INTRODUCTION

The efficient inhibition of viral infection is a major challenge for science. One approach to fight viral infection is to inhibit the virus binding to cells by competitive binding to viral proteins. Small monovalent molecules, however, have shown to be widely inefficient for this purpose. Therefore, multivalent inhibitors of different sizes and shapes, i.e., linear polymers,[1−3] dendrimers,[4−9] liposomes,[10,11] polymersomes,[12] nanogels,[13] and nanoparticles,[14−19] have been reported for the inhibition of a large variety of viruses, i.e., Influenza virus,[1,2,11,13,20,21] VSV,[22] HIV,[4,8,14,15] HSV,[17−19] or Ebola virus.[7,9] Recently we have used functionalized gold nanoparticles of different sizes for the inhibition of viral binding and infection.[20] The observed size-dependent effects were systematically studied for a more detailed understanding of multivalency effects but raised new questions as the inhibition efficiency indeed followed the trend of the contact area, but its magnitude turned out to be exceptionally larger than expected.[22] An explanation for this phenomenon as well as a general conclusion on the best size and shape for competitive binding inhibitors, however, is still lacking. The main problem is the accurate proportionate quantification of the size-dependent steric shielding and multivalency effects on the competitive binding inhibition, which are respectively the ability of inhibitors to block additional areas on the virus besides the contact area and the amplification of a binding constant due to multiple binding events.[2,10,13,22−26] Nanoparticles are especially suited for quantifying the effects as their size can be precisely varied, whereby their high symmetry facilitates geometric considerations on steric shielding. However, the virus/nanoparticle contact area (and thus the number of multiple ligand−receptor interactions) as well as the steric shielding simultaneously increase upon increasing the inhibitor size (Figure 1a). To distinguish between the size-dependent steric shielding and multivalency effects, we present here two complementary inhibition assays that are respectively based on a weak and a strong binding ligand/receptor pair (Figure 1b,c). In order to have a well-controlled and characterized system, we also have employed nanoparticles to represent viruses, which we termed "binders".

The neat size-dependent steric shielding effect was determined by using an analog of the commonly employed hemagglutination inhibition assay (Figure 1b).[22] In this assay, the binding of streptavidin functionalized, fluorescent silica nanoparticles of 192 nm (SA-NP, binders) to biotinylated

Received: November 5, 2014
Published: January 27, 2015

DOI: 10.1021/ja5114084
J. Am. Chem. Soc. 2015, 137, 2572−2579

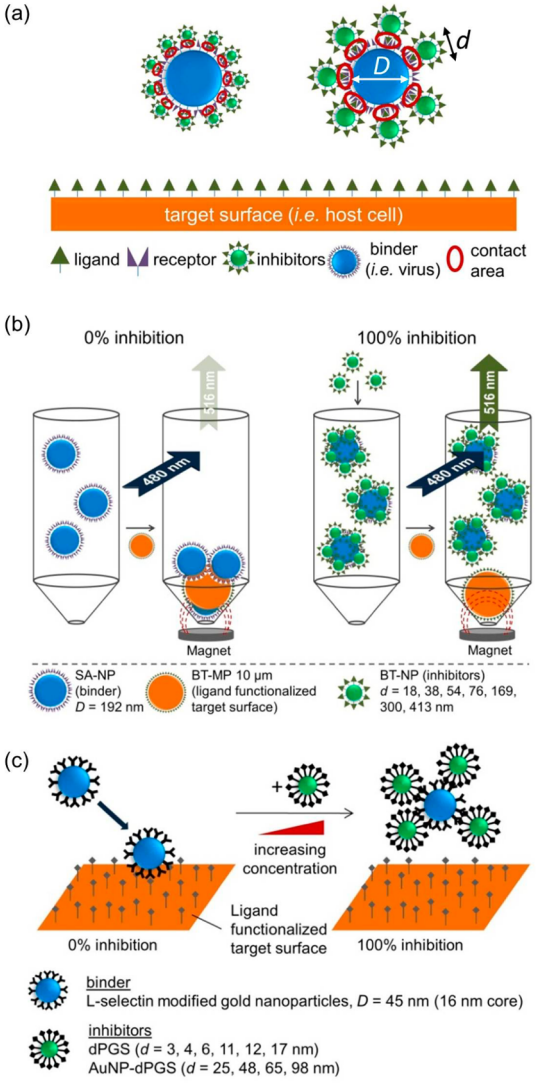

Figure 1. (a) Schematic illustration depicting the concept of virus-cell binding inhibition by globular inhibitors of different sizes. The virus/inhibitor contact area as well as the number of inhibitors required for a steric shielding of a virus depends on the inhibitor and virus sizes, denoted by d and D, respectively. (b,c) Schematic of the employed inhibition assays. (b) Fluorescence-based competitive binding inhibition assay of streptavidin functionalized, fluorescent silica nanoparticles of diameter D = 192 nm (SA-NP, binders) and biotin functionalized silica nanoparticles (BT-NP, inhibitors) with diameters d between 18 and 413 nm. The read-out was based on the fluorescence signal in the supernatant after magnetic removal of the noninhibited SA-NP with biotin functionalized magnetic particles of 10 μm (BT-MP, target surface). (c) SPR-based competitive binding inhibition assay.[27] L-selectin functionalized gold nanoparticles of diameter D = 45 nm (binders) were inhibited with dPGS (d = 3−17 nm)[28] and AuNP-dPGS (d = 25−86 nm, inhibitors), respectively.

magnetic particles of 10 μm (BT-MP, target surface) was inhibited by differently sized biotinylated silica nanoparticles (BT-NP, inhibitors). Due to the very low dissociation constant of a single streptavidin−biotin bond of approximately 10^{-15} M,[29] the multivalency effect was negligible as the dissociation constant was far below the concentration of the SA-NP. We determined the IC_{50} values for 7 differently sized BT-NP ranging from 18 nm up to 413 nm ($d < D$ and $d > D$). The changes in the inhibitor size exclusively influenced the steric shielding and therefore allowed direct quantification of this effect.

The complementary assay employed weak ligand/receptor binding pairs and was based on the respective inhibition of L-selectin (Sel) functionalized binders by dendritic polyglycerolsulfate (dPGS) derivatized scaffolds of 12 different sizes (Figure 1c). L-selectin is a cell adhesion molecule that is multivalently presented on leukocytes and initiates their recruitment from the blood flow in inflammatory processes.[30] The K_d^{mono} of this ligand/receptor pair is estimated to be in the order of 500 nM.[31] In this case, the inhibition was not only dependent on the steric shielding effect but also on the binding affinity of the inhibitor, i.e., on the inhibitor/binder contact area. Previously, we studied the binding inhibition of L-selectin functionalized 45 nm gold nanoparticles (AuNP-Sel, binder) with sulfated dendritic polyglycerol (dPGS) inhibitors.[28] The large amount of meaningful inhibition data made this assay perfectly suitable for the study of multivalency effects. As the size of the inhibitors (dPGS, 2−17 nm) did not exceed the size of the binder (AuNP-Sel, 45 nm) in this previous study, we extended our study by also measuring dPGS functionalized gold nanoparticles (AuNP-dPGS, inhibitors) in the size range of 25−98 nm.

In the present paper we demonstrate that the evaluation of the inhibition characteristics of these two assays allows a relative quantification of the steric shielding and multivalency contributions to the inhibition. The quantitative evaluation of the inhibition mechanism will (1) help one to better understand the origin of the often observed high efficacy of larger-sized inhibitors, (2) give important implications for *in vitro* testing of inhibitors, (3) permit a quantitative rating of design parameters, i.e., according to inhibitor size, inhibitor to virus contact area, and ligand density and type for the rational design of efficient inhibitors, and (4) permit prediction of the optimal inhibitor diameters for efficient treatment of viral infections.

RESULTS

The binders and inhibitors for the BT/SA and dPGS/Sel assays were characterized by DLS, TEM, and AAS measurements, respectively (Supporting Information, SI). A monomodal size distribution of low polydispersity in PBS could be confirmed for all particles. The inhibition curves obtained from the BT/SA and the dPGS/Sel assay, respectively, are presented in Figure 2.

The inhibition was plotted against the total concentration ratio of inhibitors ([I]) to binders ([B]). For the BT/SA assay (Figure 2a) steep inhibition curves were observed with 0−100% inhibition within a concentration range of 1 order of magnitude for all inhibitor diameters. Furthermore, the required concentration of BT-NPs (inhibitors) to induce comparable binding signals decreased with larger inhibitors, but the ratio of inhibitor to binder concentration at 50% inhibition generally exceeded a value of 1, even for inhibitor sizes larger than the binder size. Similar inhibition characteristics could be observed for the dPGS/Sel assay (Figure 2b). Again, the inhibitor to binder concentration ratio decreased as the inhibitor sizes increased but never fell below the value of 1 at 50% inhibition. The inhibition slope of smaller-sized dPGS-based inhibitors, however, was significantly more gentle compared to larger sized inhibitors and often required a several order of magnitude increase in particle concentration to obtain 100% inhibition.

DOI: 10.1021/ja5114084
J. Am. Chem. Soc. 2015, 137, 2572−2579

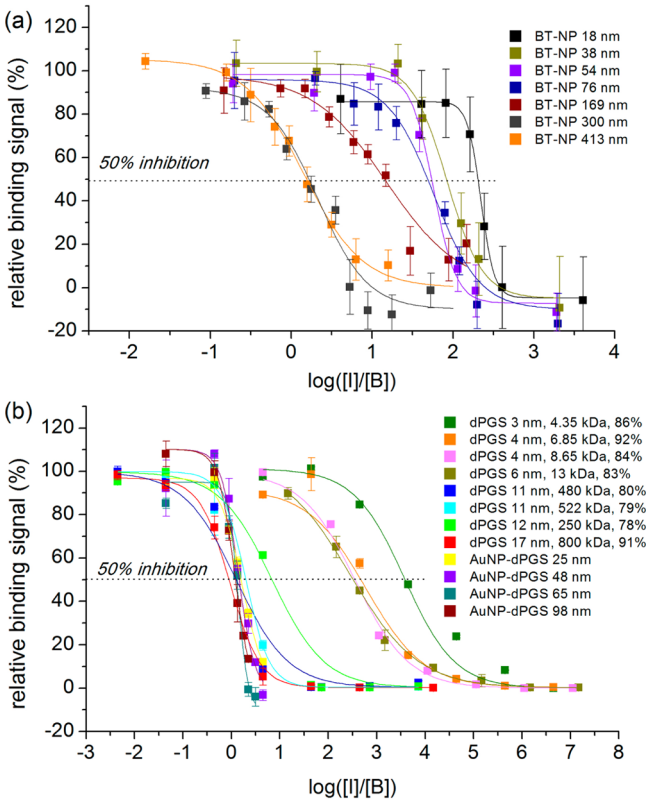

Figure 2. Relative binding signals depending on the inhibitor [I] to binder [B] concentration ratio for the (a) BT/SA and (b) dPGS/Sel assays. The binders in (a) were streptavidin functionalized, fluorescent silica nanoparticle (SA-NP) of 192 nm and in (b) AuNP-Sel of 45 nm diameter, respectively. The colored curves show the inhibition of the binders for individual inhibitor sizes. In (b), additional data are shown for corresponding molecular weights and degrees of dPGS sulfation.[28]

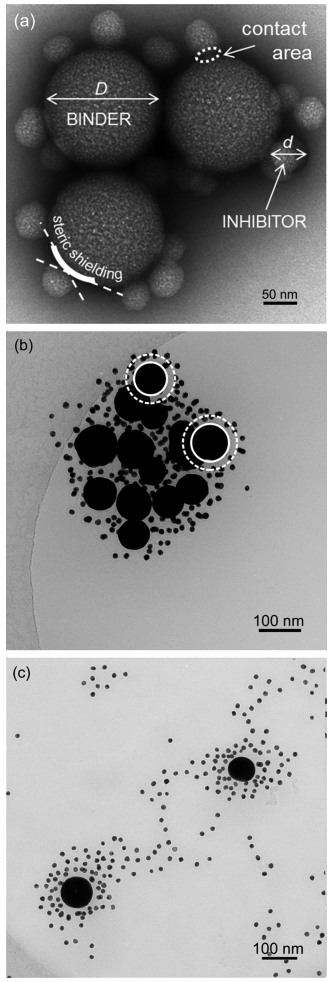

Figure 3. (a) TEM micrograph of d = 54 nm BT-NPs (inhibitors) incubated with D = 192 nm SA-NPs (binders) at a BT-NP/SA-NP concentration ratio of 15. Contact area, steric shielding area, and particle diameters are marked. (b) Cryo-TEM micrograph of d = 98 nm AuNP-dPGS (inhibitors) with D = 45 nm AuNP-Sel (16 nm gold core) (binders) at an AuNP-Sel/AuNP-dPGS concentration ratio of 30. Clustering effects are clearly visible. The corona thickness of AuNP-dPGS and AuNP-Sel of 19.4 ± 2.8 nm is indicated as determined experimentally (see SI). (c) Cryo-TEM micrograph of d = 98 nm AuNP-dPGS with D = 45 nm AuNP-Sel at an AuNP-Sel/AuNP-dPGS concentration ratio of 120. Clustering of inhibitors by binders rarely occurred.

We complemented the inhibition assays with a direct visual method by using the cryogenic transmission electron microscopy technique (cryo-TEM) for several binding inhibitors (Figure 3).

For the visualization of the binding in the BT/SA assay, we chose the 54 nm inhibitors with the 192 nm binders (Figure 3a). For the dPGS/Sel assay, we considered AuNP-dPGS (inhibitor) of 98 nm in combination with the AuNP-Sel (binder) of 45 nm (Figure 3b,c). It is obvious from the images that the distances between binders and inhibitors were rather large, which was due to the fact that strong electron scattering of metal nanoparticles prevents the visualization of low-density organic layers. A mean particle distance of 20.7 nm ±2.3 nm, however, was in good agreement with the combined contribution of AuNP-dPGS (4.5 ± 1.5 nm) and the AuNP-Sel (14.9 ± 1.3 nm) organic layers (see Figure 3b and SI).

Furthermore, clustering events of inhibitors and binders are detectable to some extent in Figure 3. The presence of clustering was therefore dependent on the employed particle ratio. Clustering was more pronounced at particle ratios at which the surface of the AuNP-dPGS was not saturated with AuNP-Sel (Figure 3b). When the binder was used in excess, clustering of inhibitors by binders did not occur (Figure 3c).

DISCUSSION

The inhibition data presented in Figure 2 indicate that there is a critical size limit for inhibitors, above which larger inhibitor size does not result in lower concentrations for inhibition. In order to better understand this phenomenon, we had to quantify the measured IC_{50} values in terms of steric shielding and multivalency effects. For this purpose, we first considered the Cheng–Prusoff equation which is commonly employed for calculating IC_{50} values depending on the concentration of a monovalent binder [B]:[32]

$$IC_{50} = K_d^{mono} + 0.5[B] \quad (1)$$

In contrast to the monovalent case, our binders were multivalent by nature, therefore the dissociation constant of the monovalent inhibitor K_d^{mono} was substituted with the effective dissociation constant of the multivalent inhibitor K_d^{multi}. Furthermore, we had to consider the number of inhibitors required to sterically shield a binder. This number is denoted as P. To draw the analogy to eq 1, we had to rescale the binder concentration with P.

DOI: 10.1021/ja5114084
J. Am. Chem. Soc. 2015, 137, 2572–2579

$$IC_{50} = \underbrace{K_d^{multi}}_{\text{multivalency contribution}} + \underbrace{0.5P[B]}_{\text{steric shielding contribution}} \quad (2)$$

A detailed derivation of eq 2 is provided in the SI. From eq 2, it is evident that the IC_{50} value splits up into a multivalency and a steric shielding term. In order to predict the steric shielding term, we started with theoretical considerations. First, it was necessary to determine the number of inhibitors P required to prevent the attachment of the binder to the target surface. Two scenarios emerged. In the first scenario, a minimum number of inhibitors arrange on the binder in order to inhibit its attachment to a planar surface (Figure 4a, P_{min}). The number of inhibitors (P_{min}) to do so is based on the ratio of the sterically shielded area (Figure 4b, area marked in red) to the overall surface area of the binder.

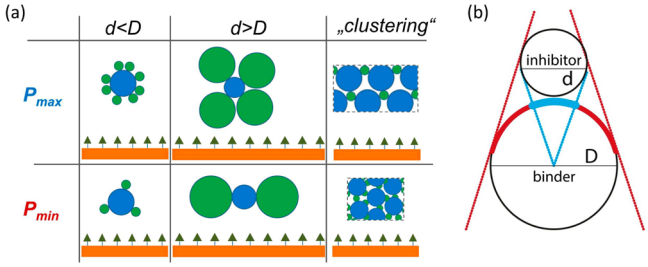

Figure 4. (a) Schematic illustration of possible arrangements for inhibitors (green) and binders (blue) depending on minimum (P_{min}) or random (P_{max}) arrangement of inhibitors on the binder. To illustrate the size dependency, selected scenarios of inhibitors smaller than binders ($d < D$) and vice versa ($d > D$) are presented. (b) Schematic illustration of the area shielded by the inhibitor on the binder. The red marking defines the area which cannot bind to a planar surface anymore (used for the calculation of P_{min}), while the blue marking defines the area which cannot bind to a second inhibitor (used for the calculation of P_{max}).

In the second scenario, inhibitors randomly arrange on the binder. The decoration is therefore more dense and irregular compared to the first case (Figure 4a, P_{max}). For the calculation of P_{max}, the area was considered which a single inhibitor needs to shield a binder surface in a projection view (Figure 4b, area marked in blue). The ratio of the binder surface area and the inhibitor shielded area, yielded values for P_{min} and P_{max}, respectively:

$$P_{min} = \frac{D}{d} + 2 \quad (3)$$

$$P_{max} = \frac{1}{1 - \sqrt{(D/d)(2 + D/d)/(1 + D/d)^2}} + 1 \quad (4)$$

Second, individual inhibitors can simultaneously bind to several binders because of their multivalent nature. This process, which we termed clustering, increases the efficiency as individual inhibitors bind to multiple binders within a cluster. The number of binders a single inhibitor can bind (M) is again dependent on the ratio of d/D:

$$M = \frac{1}{1 - \sqrt{(d/D)(2 + d/D)/(1 + d/D)^2}} + 1 \quad (5)$$

M was calculated in an analogous manner described for P_{max} (eq 4). Combining P with M allows one to describe clustering according to the employed decoration models:

$$P_{min,cluster} = \left(\frac{D}{d} + 2\right)/M \quad (6)$$

$$P_{max,cluster} = \left(\frac{1}{1 - \sqrt{(D/d)(2 + D/d)/(1 + D/d)^2}} + 1\right)/M \quad (7)$$

From eq 2 it follows that the number of inhibitors required to fully inhibit a binder P can be directly obtained from the measured IC_{50} value, if the dissociation constant K_d^{multi} is very low ($K_d^{multi} \ll 0.5P[B]$). In this limit P reads:

$$P = \frac{2 \cdot IC_{50}}{[B]} \quad (\text{if } K_d^{multi} \ll 0.5P[B]) \quad (8)$$

In Figure 5 the experimentally obtained P value according to eq 8 is compared to the theoretical values of P_{min} and P_{max} (eqs 3 and 4), respectively.

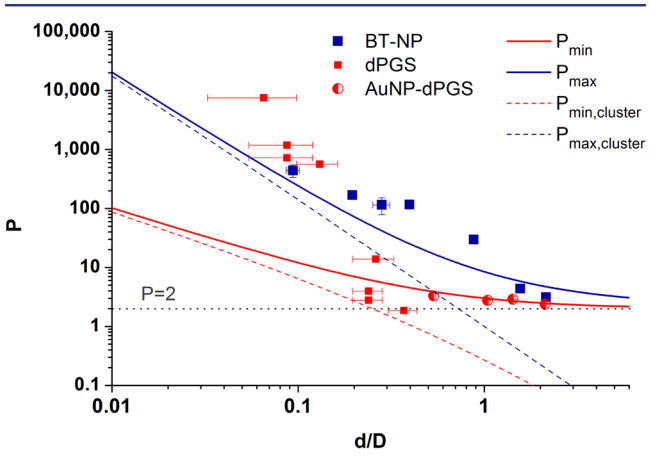

Figure 5. Combination of the experimental and theoretical numbers of inhibitors P required to inhibit the binding of a binder to a planar surface. The data points depicting the experimental data are colored in red for the dPGS/Sel assay and in blue for the BT/SA assay, respectively, as determined by eq 8. The dashed and continuous lines represent the predicted values based on the theoretical models for P_{max} and P_{min} with (eqs 6 and 7) and without (eqs 3 and 4) clustering, respectively. The dotted gray line marks the situation for an inhibitor/binder ratio of two ($P = 2$).

The experimental data from the BT/SA-based assay (Figure 5) are best described by the theoretical curve progression of P_{max}, which implies a random packing of the inhibitors on the binder (Figure 4a). We assume that the high packing density of BT-NP is caused by the absence of charges (= absence of interparticle repulsion) which is confirmed by a random packing of BT-NP observed by TEM (Figure 3a). The fact that P is larger than two even at very large d/D ratios of 1.5 and 2.2 (corresponding to 300 and 413 nm sized BT-NPs) is an indication that clustering does not have a major quantitative impact on the inhibition. As the inhibitors of the BT/SA assays inhibit according to the theoretical model for steric shielding with ($P = P_{max}$), the complete binding of all inhibitors to the binder was confirmed.

A similar trend was observed with the experimental data of the dPGS/Sel assay. P never fell below a value of 2, which again supports the finding that the formed clusters are of minor impact. The experimental data for d/D ratios of 0.3−2 from the dPGS/Sel assay, however, follow a different trend if compared to the BT/SA assay. They are best described by the course of P_{min}, which indicates a much lower packing density of the

DOI: 10.1021/ja5114084
J. Am. Chem. Soc. 2015, 137, 2572−2579

inhibitors on the binder surface (Figure 4a). We assume that this difference is due to the highly charged nature of the AuNP-dPGS which results in electrostatic repulsion of the nanoparticles, and hence causes a lower packing density. Furthermore, the correspondence of P with P_{min} required at d/D ratios above 0.3 implies that all inhibitors are ratnd to the AuNP-Sel. This strong binding was confirmed by cryo-TEM, which showed almost no unbound AuNP-Sel particles (Figure 3b). For all ratios below d/D = 0.3, the experimental data exhibited a significant deviation from P_{max} as well as P_{min}. We assume that this phenomenon was due to an increase of K_d^{multi} for smaller inhibitors. In order to clarify this we further investigated the IC_{50} values (Figure 6).

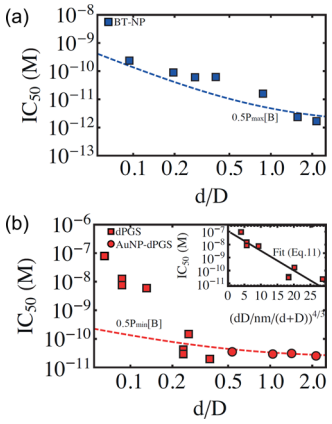

Figure 6. IC_{50} values determined from (a) BT/SA and (b) dPGS/Sel assays, respectively. The corresponding dashed lines mark IC_{50} values under the assumption that inhibitors bind completely to the binders with $0.5P_{max}[B]$ for (a) and $0.5P_{min}[B]$ for (b), respectively. The inset diagram in (b) denotes the fit of the dPGS data to eq 11 with K_d^{mono} = 94 nM and γ = 0.34 $nm^{-4/3}$.

For the BT/SA assay, the measured IC_{50} values were equivalent to the course of $0.5P_{max}[B]$ (Figure 6a), which indicates that $K_d^{multi} \ll 0.5P_{max}[B]$ (see eq 2). Hence, the observed changes in the IC_{50} values for differently sized inhibitors were only based on steric shielding effects. This was expected, as the $K_d^{mono}$of BT/SA is approximately 10^{-15} M,[29] i.e., several orders of magnitude lower than the concentration of SA-NPs (binders) in the assay with [B] = 1.13 pM.

For the dPGS/Sel-based assay, however, we observed a different trend (Figure 6b). For smaller dPGS ($d/D < 0.3$), the measured IC_{50} values were much higher than $0.5P_{min}[B]$. Thus, the multivalent dissociation constants can be directly obtained in this regime from the IC_{50} values.

Before we discuss the size dependency of the dissociation constants, we will briefly present a motivation for a heuristic equation for K_d^{multi}. Starting from the dissociation constant of a monovalent ligand/receptor pair $K_d^{mono} = V \exp[-\Delta G/k_BT]$ (with ΔG the binding free energy of a monovalent ligand/receptor pair, k_BT as the thermal energy, and V a measure for the volume of the binding site) the multivalent dissociation constant reads:

$$K_d^{multi} = V\exp\left[-\alpha\frac{\Delta G \cdot N}{kT}\right] = K_d^{mono}\exp\left[-\frac{\Delta G}{kT}(\alpha N - 1)\right] \quad (9)$$

with α the so-called cooperativity factor and N the number of interacting ligand/receptor pairs.[24] Furthermore, we assume that N is proportional to the contact area (A_c) between binder and inhibitor. According to the JKR model,[33] which describes the relationship between the contact area of two elastic, adhesive spheres and the diameters of the spheres, d and D, respectively, the contact area is given by

$$A_c = 2\pi\left(\frac{6\pi g}{K}\right)^{2/3}\left(\frac{dD}{d+D}\right)^{4/3} \quad (10)$$

with g the binding energy per unit area and K the effective elastic constant. In the limit of a very large number of interaction ligand/receptor pairs ($N \gg 1$) K_d^{multi} reads:

$$K_d^{multi} \approx K_d^{mono}\exp\left[-\frac{\Delta G}{kT}\alpha N\right] = K_d^{mono}\exp\left[-\gamma\left(\frac{dD}{d+D}\right)^{4/3}\right] \quad (11)$$

Equation 11 describes the experimental data well with K_d^{mono} = 94 nM and γ = 0.34 $nm^{-4/3}$ (Figure 6b, inset). For example, Woelke et al. showed that the sulfate-dependent dissociation constant toward L-selectin is approximately 500 nM,[31] thus the experimentally determined monovalent dissociation constant is reasonable (Figure 6b, inset). Furthermore, the exponential dependence of K_d^{multi} on N is in good agreement with a previous study by Hong et al.,[34] which reported an exponential relationship for the binding of nanoparticles of varied ligand densities at a fixed diameter to multivalent surfaces. In eq 11, the ligand density is incorporated in γ, which we term amplification factor. Furthermore, the factor γ includes the deformability of the inhibitor as well as cooperative effects. The deformability and ligand density of the inhibitors employed in the presented assays can be assumed to be nearly constant. Even though the magnitude of cooperative effects cannot be determined, the ability to exponentially fit the K_d^{multi} using a constant prefactor indicates that cooperative effects are constant over the entire range of inhibitor sizes.

Now, the various factors affecting the IC_{50} values of globular inhibitors can be put in order. IC_{50} values are most of all dependent on the inhibitor/binder contact area and the ligand density, as both correlate with N and therefore, have an exponential influence on the K_d^{multi} value (eq 11), which itself directly correlates with the IC_{50} value (eq 2). Due to the relationship of contact area and inhibitor diameter d (eq 10), IC_{50} values also decrease exponentially with the inhibitor size. Nevertheless, the benefit of the inhibitor potential by multivalency is only measurable as long as $K_d^{multi} \gg 0.5P[B]$. If $K_d^{multi} \ll 0.5P[B]$, all inhibitors bind completely to the binders and a further increase of the contact area or ligand density does not have any measurable effect on the IC_{50} values. A further increase of the inhibitor diameter therefore lowers the IC_{50} value only because of the enhanced steric shielding effect. Compared to the exponential dependence of the IC_{50} values on the inhibitor size because of multivalency, the impact of the inhibitor size on steric shielding and therefore, the IC_{50} values, is relatively weak. Hence, the many reported extremely low IC_{50} values of ligand decorated globular scaffolds,[6,10−13,15,20,22] can now be identified to be predominantly based on multivalency effects. A more detailed discussion about the impact of eq 2 on the prediction of the IC_{50} values of globular inhibitors is given in the SI.

The Optimal Inhibitor Size. For applications, the prediction of the "optimal inhibitor size" is often desirable. In terms of inhibitor efficiency, the optimal inhibitor size might be best determined by the lowest mass concentration of the inhibitor. For a general prediction of the optimal size of a globular inhibitor independently of the scaffold material, the

DOI: 10.1021/ja5114084
J. Am. Chem. Soc. 2015, 137, 2572−2579

consideration of the volume normalized concentration (which correlates with the mass normalized concentration) is better suited as it permits the comparison of inhibitors of different materials. The volume normalization of the inhibition data can be performed by the multiplication of P (Figure 5) at a specific d/D ratio by the factor $(d/D)^3$, respectively (Figure 7a).

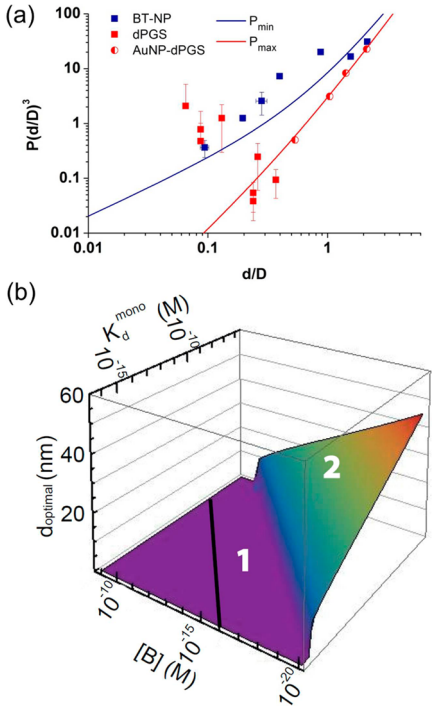

Figure 7. (a) Combination of the experimental and theoretical volume normalized number of inhibitors, $P(d/D)^3$, required to inhibit a binder from attaching to a planar surface. The data points depicting the experimental data are colored in red for the dPGS/Sel assay and in blue for the BT/SA assay, respectively. The continuous lines represent the predicted values based on the theoretical models for P_{max} and P_{min}. (b) Predicted d/D ratios for globular inhibitors which result in the lowest required volume concentration of inhibitors to reduce the binding of a hypothetical binder (D = 100 nm) to its target surface by 50% in dependence on K_d^{mono} and the binder concentration [B]. The graph can be divided into regimes (1) in which even for the smallest possible inhibitor size a complete binding to the binder is observed and (2) in which larger inhibitor diameters are required for a complete binding of all inhibitors. The black solid line marks K_d^{mono} = [B].

The volume normalized values $P(d/D)^3$ which were calculated by the models for steric shielding, both increase with higher d/D ratios. Therefore, increasing the size of inhibitors which bind completely to the binder ($K_d^{multi} \ll 0.5P[B]$) is always disadvantageous, as higher mass concentrations have to be applied for inhibition. This could be confirmed by examining the BT/SA assay data (Figure 7a, BT-NP). For the dPGS/Sel assay, the same effect could be observed for larger AuNP-dPGS (d/D > 0.3), which was expectable as the particles were shown to bind completely to the binders (Figure 3b,c). However, for smaller sized dPGS (d/D < 0.3), $P(d/D)^3$ decreased with increasing d/D ratios. A minimum of $P(d/D)^3$ was approached at a d/D ratio of ~0.3. At this inhibitor size, the lowest volume and therefore mass of the inhibitors is required for inhibition. The presence of an optimum inhibitor diameter can be best described by eq 12, which is a combination of eq 2 and 11:

$$IC_{50}d^3 = K_d^{mono} e^{[-\gamma(dD/d+D)^{4/3}]} d^3 + 0.5P[B]d^3 \quad (12)$$

P corresponds to P_{min} and P_{max} for charged and neutral inhibitors, respectively. The lower the value of $IC_{50}d^3$ of an inhibitor of diameter d, the less volume concentration has to be applied for 50% inhibition. Independently of the steric shielding model applied (P_{min} or P_{max}), the value of the steric shielding term always increases faster with the inhibitor diameter d than the cubic increase in volume. Therefore, increasing the size of inhibitors which bind completely to the inhibitors, i.e., BT-NP or AuNP-dPGS with a d/D ratio > 0.3 always results in higher inhibitor volume concentrations at 50% inhibition. However, the value of the multivalency term always decreases faster than d^3. Hence, for inhibitors which do not bind completely to the target ($K_d^{multi} \gg 0.5P[B]$), larger inhibitors always result in lower volumes at the IC_{50} concentration until a d/D ratio is approached at which $K_d^{multi} \approx 0.5P[B]$. At this ratio, e.g., 0.3 for the dPGS/Sel assay (Figure 7a), inhibitors bind completely to the binder and multivalency effects are negligible.

Equation 12 summarizes all the above-discussed factors, which determine the required volume concentration of a globular inhibitor needed for 50% inhibition. For most applications, however, the investigator knows the binder, i.e. virus, diameter, and the K_d^{mono} of the employed ligand. To highlight the importance of the binder concentration for the rational design of competitive binding inhibitors, we predicted the optimal diameter for the inhibition of a hypothetical binder (D = 100 nm) by a globular binding inhibitor in dependence of K_d^{mono} and [B] (Figure 7b).

For the prediction, we employed the same prefactor as determined for the dPGS/Sel assay (γ = 0.34 nm$^{-4/3}$) and the P_{max} values appropriate for neutral inhibitors. The plot in Figure 7b is clearly divided into two regimes, namely regime (1) in which even for smallest inhibitor sizes $K_d^{multi} \leq 0.5P[B]$, and regime (2) in which larger inhibitor diameters are required for $K_d^{multi} \approx 0.5P[B]$, respectively. In the case of regime (1), where even the smallest inhibitors all bind completely to the binder, the dependence of the volume concentration at the IC_{50} is mainly based on the steric shielding, whereupon larger inhibitors give higher volume concentrations. Thus, the multivalent presentation of ligands in regime (1) on globular inhibitors is disadvantageous. In regime (2), the volume concentration at 50% inhibition is mainly dictated by multivalency effects. As the exponential scale of the multivalency term is much larger than the cubic increase in volume, larger inhibitors are always favored up to the optimum d/D ratio for which $K_d^{multi} \approx 0.5P[B]$ holds. Thus, depending on the concentration of the binder in the application, even for very strong binding ligand/receptor pairs, e.g., antibodies, the multivalent presentation of the ligands on a globular scaffold can be advantageous. Nevertheless, as K_d^{multi} exponentially increases with larger inhibitor sizes, a complete binding of inhibitors to the binder is given at an inhibitor diameter of 45 nm (d/D = 0.45) even for a very low binder concentration of 10^{-20} M and a K_d^{mono} of 10^{-6} M. Therefore, the optimum inhibitor size for the considered conditions is always smaller than the binder itself.

Just like the amplification factor, the binder diameter dictates the inhibitor/binder contact area and therefore has an exponential influence on the optimal inhibitor diameter at specific K_d^{mono} and [B]. Counterintuitively, the optimal inhibitor sizes for the inhibition of larger binders in comparison to smaller binders have to be lower at the same concentration, as

DOI: 10.1021/ja5114084
J. Am. Chem. Soc. 2015, 137, 2572−2579

increasing the size of the binder also increases the inhibitor/binder contact area (Figure S11). With lower amplification factors and therefore lower ligand densities, larger inhibitor diameters are favored as a complete binding of the inhibitors takes more contact area (Figure S10). The model for steric shielding (P_{min}/P_{max}) has only a minor impact on the optimal inhibitor diameter and is therefore largely irrelevant for applications (Figure S12).

Interestingly, we have predicted optimal inhibitor diameters larger than the binder only in those cases where very low ligand densities or very small binders (<50 nm) prevailed (SI). Therefore, inhibitor diameters below the size of the binder are advantageous in most cases. From the experimental data of the dPGS/Sel and BT/SA inhibition assays, we validated the above findings for binder diameters of 46 and 192 nm, respectively (Figure S13). Since the experimental conditions for the BT/SA assay were clearly in regime (1), the optimal inhibitor should be as small as possible (Figure 7a). The experimental conditions for the dPGS/Sel assay were in regime (2) with an optimal d/D ratio of 0.3 (Figure 7a).

CONCLUSION

The quantification of the steric shielding and multivalency contributions on the IC_{50} values of differently sized globular binding inhibitors provides useful guidelines for the design of competitive binding inhibitors. The particle and volume normalized IC_{50} value of an inhibitor at very low binder concentrations [B] predominantly depends on its multivalent dissociation constant K_d^{multi}. The K_d^{multi} and thus the IC_{50} values show an exponential dependence on the inhibitor/binder contact area. Hence, the IC_{50} values of larger sized inhibitors are often observed to be several orders of magnitude lower compared to the monovalent ligand.[4,5,10−13,20] As the increase in contact area with inhibitor size levels off for binder-sized inhibitors, this effect is more pronounced at lower inhibitor/binder size ratios. Compared to the multivalency effects, the contribution of steric shielding to the IC_{50} values of inhibitors is only minor, and its impact is only noticeable if $K_d^{multi} \ll 0.5P[B]$, meaning if all inhibitors are bound to the binder. In this case, an increase in inhibitor size is unfavorable, as the volume and therefore mass of the inhibitor increases faster with inhibitor size than the steric shielding contribution. Most importantly, it is necessary to emphasize the dependence of the predominant effect (steric shielding or multivalency, respectively) on the binder concentration. Because of the exponential dependence of K_d^{multi} on the contact area, especially larger sized inhibitors often have multivalent dissociation constants far below the experimental binder, i.e., virus, concentration so that only steric shielding effects can be observed. The concentration of viruses in the body fluids of infected individuals is often several order of magnitudes lower, in which case lower K_d^{multi} (meaning larger inhibitors and/or higher ligand functionalization) would be of major advantage. Because of the quantitative relationship between inhibitor volume, multivalency effects, and steric shielding, the optimal size of a globular inhibitor for the lowest volume normalized IC_{50} value provides just enough contact area for inhibitors to bind completely to the binder at the given binder concentration. Our predictions show that optimal inhibitor diameters are in most cases smaller than the binder itself.

Besides globular inhibitors, sheet-like inhibitors should have a very high potential. They provide very large contact areas at low volumes, which is a prerequisite for efficient volume normalized inhibition. In future projects, we will adopt our model for competitive binding inhibition to other geometrical structures to facilitate the rational design of competitive binding inhibitors for the efficient treatment of viral diseases.

ASSOCIATED CONTENT

Supporting Information

Experimental section, derivation of geometric models, characterization of nanoparticles, additional formulas and instructions for application. This material is available free of charge via the Internet at http://pubs.acs.org.

AUTHOR INFORMATION

Corresponding Authors

*jonathan.vonnemann@chemie.fu-berlin.de
*sliese@zedat.fu-berlin.de

Notes

The authors declare no competing financial interest.

ACKNOWLEDGMENTS

This contribution was generously supported by the Deutsche Forschungsgemeinschaft DFG by grants to the SFB 765 and the Core Facility BioSupraMol (www.biosupramol.de). The Focus Area Nanoscale of the Freie Universität Berlin (www.nanoscale.fu-berlin.de) is acknowledged for the practical and technical support.

REFERENCES

(1) Lees, W. J.; Spaltenstein, A.; Kingery-Wood, J. E.; Whitesides, G. M. *J. Med. Chem.* **1994**, *37*, 3419.
(2) Sigal, G. B.; Mammen, M.; Dahmann, G.; Whitesides, G. M. *J. Am. Chem. Soc.* **1996**, *118*, 3789.
(3) Lüscher-Mattli, M. *Antivir. Chem. Chemother.* **2000**, *11*, 249.
(4) Price, C. F.; Tyssen, D.; Sonza, S.; Davie, A.; Evans, S.; Lewis, G. R.; Xia, S.; Spelman, T.; Hodsman, P.; Moench, T. R.; Humberstone, A.; Paull, J. R. a; Tachedjian, G. *PLoS One* **2011**, *6*, e24095.
(5) Rupp, R.; Rosenthal, S. L.; Stanberry, L. R. *Int. J. Nanomed.* **2007**, *2*, 561.
(6) Bourne, N.; Stanberry, L. R.; Kern, E. R.; Holan, G.; Bernstein, D. I. *Antimicrob. Agents Chemother.* **2000**, *44*, 2417.
(7) Arce, E.; Otero, J. R.; Rojo, J.; Delgado, R. *Antimicrob. Agents Chemother.* **2003**, *47*, 3970.
(8) Choopanya, K.; Martin, M.; Suntharasamai, P.; Sangkum, U.; Mock, P. A.; Leethochawalit, M.; Chiamwongpaet, S.; Kitisin, P.; Natrujirote, P.; Kittimunkong, S.; Chuachoowong, R.; Gvetadze, R. J.; McNicholl, J. M.; Paxton, L. A.; Curlin, M. E.; Hendrix, C. W.; Vanichseni, S. *Lancet* **2013**, *381*, 2083.
(9) Luczkowiak, J.; Sattin, S.; Sutkevi, I.; Reina, J.; Macarena, S.; Martínez-prats, L.; Daghetti, A.; Fieschi, F.; Delgado, R.; Bernardi, A.; Rojo, J. *Bioconjugate Chem.* **2011**, *22*, 1354.
(10) Kingery-wood, J. E.; Williams, K. W.; Sigal, G. B.; Whitesides, G. M. *J. Am. Chem. Soc.* **1992**, *114*, 7303.
(11) Spevak, W.; Nagy, J. O.; Charych, D. H.; Schaefer, M. E.; Gilbert, J. H.; Bednarski, M. D. *J. Am. Chem. Soc.* **1993**, *115*, 1146.
(12) Nazemi, A.; Haeryfar, S. M. M.; Gillies, E. R. *Langmuir* **2013**, *29*, 6420.
(13) Papp, I.; Sieben, C.; Sisson, A. L.; Kostka, J.; Böttcher, C.; Ludwig, K.; Herrmann, A.; Haag, R. *ChemBioChem* **2011**, *12*, 887.
(14) Date, A. A.; Destache, C. J. *Biomaterials* **2013**, *34*, 6202.
(15) Bowman, M.-C.; Ballard, T. E.; Ackerson, C. J.; Feldheim, D. L.; Margolis, D. M.; Melander, C. *J. Am. Chem. Soc.* **2008**, *130*, 6896.
(16) Di Gianvincenzo, P.; Marradi, M.; Martínez-Avila, O. M.; Bedoya, L. M.; Alcamí, J.; Penadés, S. *Bioorg. Med. Chem. Lett.* **2010**, *20*, 2718.
(17) Baram-Pinto, D.; Shukla, S.; Perkas, N.; Gedanken, A.; Sarid, R. *Bioconjugate Chem.* **2009**, *20*, 1497.

DOI: 10.1021/ja5114084
J. Am. Chem. Soc. 2015, 137, 2572−2579

(18) Baram-Pinto, D.; Shukla, S.; Gedanken, A.; Sarid, R. *Small* **2010**, *6*, 1044.
(19) Orlowski, P.; Tomaszewska, E.; Gniadek, M.; Baska, P.; Nowakowska, J.; Sokolowska, J.; Nowak, Z.; Donten, M.; Celichowski, G.; Grobelny, J.; Krzyzowska, M. *PLoS One* **2014**, *9*, e104113.
(20) Papp, I.; Sieben, C.; Ludwig, K.; Roskamp, M.; Böttcher, C.; Schlecht, S.; Herrmann, A.; Haag, R. *Small* **2010**, *6*, 2900.
(21) Waldmann, M.; Jirmann, R.; Hoelscher, K.; Wienke, M.; Niemeyer, F. C.; Rehders, D.; Meyer, B. *J. Am. Chem. Soc.* **2014**, *136*, 783.
(22) Vonnemann, J.; Sieben, C.; Wolff, C.; Ludwig, K.; Böttcher, C.; Herrmann, A.; Haag, R. *Nanoscale* **2014**, *6*, 2353.
(23) Choi, S. K.; Mammen, M.; Whitesides, G. M. *Chem. Biol.* **1996**, *3*, 97.
(24) Mammen, M.; Choi, S.-K.; Whitesides, G. M. *Angew. Chem., Int. Ed.* **1998**, *37*, 2754.
(25) Martínez-, O.; Hijazi, K.; Marradi, M.; Clavel, C. *Chem.—Eur. J.* **2009**, *15*, 9874.
(26) Reuter, J. D.; Myc, a; Hayes, M. M.; Gan, Z.; Roy, R.; Qin, D.; Yin, R.; Piehler, L. T.; Esfand, R.; Tomalia, D. a; Baker, J. R. *Bioconjugate Chem.* **1999**, *10*, 271.
(27) Dernedde, J.; Rausch, A.; Weinhart, M.; Enders, S.; Tauber, R.; Licha, K.; Schirner, M.; Zügel, U.; von Bonin, A.; Haag, R. *Proc. Natl. Acad. Sci. U. S. A.* **2010**, *107*, 19679.
(28) Weinhart, M.; Gröger, D.; Enders, S.; Riese, S. B.; Dernedde, J.; Kainthan, R. K.; Brooks, D. E.; Haag, R. *Macromol. Biosci.* **2011**, *11*, 1088.
(29) Chaiet, L.; Wolf, F. J. *Arch. Biochem. Biophys.* **1964**, *106*, 1.
(30) Ley, K.; Laudanna, C.; Cybulsky, M. I.; Nourshargh, S. *Nat. Rev. Immunol.* **2007**, *7*, 678.
(31) Woelke, A. L.; Kuehne, C.; Meyer, T.; Galstyan, G.; Dernedde, J.; Knapp, E.-W. *J. Phys. Chem. B* **2013**, *117*, 16443.
(32) Cheng, Y.-C.; Prusoff, W. H. *Biochem. Pharmacol.* **1973**, *22*, 3099.
(33) Johnson, K. L.; Kendall, K.; Roberts, A. D. *Proc. R. Soc. London A* **1971**, *324*, 301.
(34) Hong, S.; Leroueil, P. R.; Majoros, I. J.; Orr, B. G.; Baker, J. R.; Banaszak Holl, M. M. *Chem. Biol.* **2007**, *14*, 107.

DOI: 10.1021/ja5114084
J. Am. Chem. Soc. 2015, 137, 2572−2579